

## Article

# Design and Rapid Prototyping of 3D-Printed Microfluidic Systems for Multiphase Flow

Bastian Oldach , Robin Fortmann , Theo Pleie, Philip Timm and Norbert Kockmann \* 

Laboratory of Equipment Design, Department of Biochemical and Chemical Engineering, TU Dortmund University, Emil-Figge-Straße 68, 44227 Dortmund, Germany; bastian.oldach@tu-dortmund.de (B.O.); robin.fortmann@tu-dortmund.de (R.F.); theo.pleie@tu-dortmund.de (T.P.); philip.timm@tu-dortmund.de (P.T.)

\* Correspondence: norbert.kockmann@tu-dortmund.de; Tel.: +49-(0)-231-755-8077

**Abstract:** Since the emergence of microfluidic devices, subtractive manufacturing techniques have dominated their production. Although the conventional manufacturing processes are well established, they come along with some disadvantages that limit the accessibility and hinder the further development of microfluidics. With the rise of additive manufacturing, researchers are focused on developing alternative fabrication methods to promote affordability and accessibility. This paper presents the opportunities and challenges of laser-based stereolithography printers for the fabrication of microfluidic equipment. Emphasis is put on the design and iterative prototyping process from the initial design idea to the final device. To print with adequate and sufficient geometrical accuracy and suitable material, the optimization of the printer's performance is discussed. Regarding the design of multiphase microfluidics and its complex fluid behavior, suitable surface treatments, including an appropriate cleaning protocol, and coating strategies to make the printed channels either hydrophilic or hydrophobic are presented to ensure applicability. With these fundamentals of additive manufacturing in microfluidic fabrication at hand, the second focus of this contribution is on the application of a modular co-flow device and a monolithic flow-focusing device to generate droplets and slugs in different multiphase flow applications. The presented co-flow setup features a tapered capillary that affects the droplet and slug sizes due to differing diameters, with larger diameters leading to larger droplets and slugs and vice versa. Several design parameters for the flow-focusing device were evaluated to determine the influence of device design on multiphase flow formation. It was found that the diameter of the inlet for the dispersed phase has the greatest effect on the size of the resulting droplets and slugs and covers the largest range of adjustable sizes.

**Keywords:** microstructured devices; microfluidics; additive manufacturing; stereolithography; droplets; design thinking; rapid prototyping



**Citation:** Oldach, B.; Fortmann, R.; Pleie, T.; Timm, P.; Kockmann, N. Design and Rapid Prototyping of 3D-Printed Microfluidic Systems for Multiphase Flow. *Chemistry* **2024**, *6*, 1458–1476. <https://doi.org/10.3390/chemistry6060088>

Academic Editors: Igor Alabugin and Valentine Vullev

Received: 16 October 2024

Revised: 14 November 2024

Accepted: 19 November 2024

Published: 21 November 2024



**Copyright:** © 2024 by the authors. Licensee MDPI, Basel, Switzerland. This article is an open access article distributed under the terms and conditions of the Creative Commons Attribution (CC BY) license (<https://creativecommons.org/licenses/by/4.0/>).

## 1. Introduction

Systems that process or manipulate small volumes of fluids, designated as microfluidics, have revolutionized various scientific fields such as biology, chemistry, and medicine in the last decades [1–4]. The emergence of microfluidics can be traced back to the miniaturization trend in analytical chemistry leading to micro total chemical analysis systems ( $\mu$ TASs), which was mainly influenced by advances in micro-electromechanical systems (MEMS) [5,6]. By manipulating fluids on the microscale, eminent control and precision enable innovation in diagnostics, analytics, drug development, and life sciences [7–9].

The rise of microfluidics can be attributed to its potential to perform complex biochemical and chemical processes with minimal sample volumes, reduced reagent consumption, and faster reaction times [10,11]. Early microfluidic systems include inkjet printheads and DNA chips, but they have quickly expanded to a wide range of applications. The great potential of microfluidics lies in its ability to integrate multiple laboratory

functions on a single chip, often referred to as a lab-on-a-chip (LOC) [12]. The integration facilitates high-throughput screening, point-of-care diagnostics, and environmental monitoring, among other applications [10,13,14].

An important field of microfluidics is the application of multiphase flows, which involve the simultaneous flow of two or more immiscible fluids [15,16]. In microfluidic systems, multiphase flows can be used to create droplets, bubbles, and emulsions with highly controlled sizes and compositions, which offer unique opportunities for scientific and technological progress [17]. These segmented flows can be achieved via different flow devices that affect the flow formation due to their geometries and dimensions. The most common ones are cross-flow, co-flow, and flow-focusing setups. Droplets or bubbles can serve as individual microreactors, allowing for high-throughput screening and the study of reactions under well-defined conditions [10,11,18]. Furthermore, the precise control of droplet formation and manipulation simplifies the study of fluid dynamics, interfacial phenomena, and the behavior of complex fluids at the microscale [19,20]. The capabilities of controlled multiphase flows are particularly useful in applications such as drug delivery, material synthesis, chemical reactions, and biological assays, enabling the compartmentalization and isolation of reactions in small volumes [21–23]. However, the difficulty of manufacturing microfluidic devices prevented rapid development for a long time, as the high costs and the required expertise limited the access to these devices to a select group of people.

The manufacturing techniques for microfluidic devices have evolved significantly over the past few years [24–27]. Initially, photolithography, with its origin in the semiconductor industry, was the primary fabrication method [28]. However, the associated materials feature some relevant drawbacks, as silicon is expensive and cannot be coupled to optical microscopy because of its opaqueness, and both silicon and glass have low gas permeability, which makes them inappropriate for its use in biotechnology. In the late 1980s, researchers were devoted to expanding microscale production to transparent, flexible, cheap, and easy-to-process materials. One of the influential accomplishments in the field of microfluidics was the development of soft lithography and its application to polydimethylsiloxane (PDMS) by Prof. G. M. Whitesides, to whom this Special Issue is dedicated, and his laboratory at Harvard University in the late 1990s and early 2000s [29–32]. PDMS is a silicon-based organic polymer that meets these requirements, making it ideal for a wide range of microfluidic applications. This technique democratized the fabrication process as it addressed some of the previous limitations, making it more accessible to researchers worldwide and allowing for the rapid and cost-effective production of microfluidic devices, leading to fast innovation [29]. As PDMS soft lithography is also capable of combining multiple layers with more complex geometries and functionalities, it can also be considered an early predecessor of layer-by-layer production as used in modern 3D printers [33–35]. Whitesides' work in soft lithography and microcontact printing laid the foundation for many of the techniques and approaches used in microfluidic device fabrication today. His emphasis on simplicity, affordability, and accessibility has guided much of the research and development in this area.

In recent years, additive manufacturing, commonly known as 3D printing, has been trending as a fabrication method to produce microfluidic systems [36–39]. Three-dimensional printing techniques such as stereolithography (SLA), fused filament fabrication (FFF), and digital light processing (DLP) offer several advantages over traditional fabrication methods, including the ability to create complex geometries, reduce material waste, simplicity, and produce devices rapidly and cost-effectively. Besides the reduced material costs, the acquisition costs of the necessary equipment are low as well. Furthermore, saving the designs as computer-aided design (CAD) files and a fast-growing community allow for cloud manufacturing. The improved accessibility provided by 3D printing is helping microfluidics to find its way into more labs [40]. The state-of-the-art fabrication of 3D-printed microfluidics is primarily focused on SLA and FFF fabrication, with both featuring unique chances but also challenges, which include material compatibility, surface quality



and properties, and the realization from initial idea to a functional device. The promising trend requires the standardization of 3D printing methods and design guidelines that are particularly suitable for researchers new to the field to further promote research in microfluidics [40,41].

The layer-by-layer production enables the creation of entangled microfluidic channels and components that would be challenging or impossible to fabricate using conventional methods. The versatility of 3D printing also allows for the integration of multiple materials and functionalities into a single device. For instance, researchers have developed 3D-printed microfluidic systems with embedded sensors, valves, and other active components, paving the way for more sophisticated and multifunctional LOC devices. The ability to rapidly prototype and iterate designs using 3D printing accelerates the development cycle, facilitating the exploration of new concepts and applications in microfluidics [39,42,43].

Rapid prototyping and design thinking are key components in the development of microfluidic systems. Rapid prototyping, enabled by inexpensive and fast fabrication techniques, allows researchers to quickly create and test new designs, identify potential issues, and make necessary modifications. This iterative process is essential for enhancing device performance, optimizing functionality, and reducing time to market [42–44]. Design thinking is a systematic approach for innovation that emphasizes feasibility, viability, and desirability [45]. In the context of microfluidics, design thinking involves understanding the needs and constraints of end-users, whether they are researchers, users, or people in need, and designing devices that effectively address those needs. This approach encourages multidisciplinary collaboration, bringing together expertise from fields such as engineering, biology, chemistry, and medicine to create integrated and purposefully microfluidic systems. The combination of rapid prototyping and design thinking promotes the development and innovation of microfluidic devices that are not only technically advanced but also suitable for everyday use.

The rise and quick development of additive manufacturing techniques are currently causing a paradigm shift in the state-of-the-art fabrication of microfluidics. The simplicity, affordability, and accessibility promote the further and more rapid development of microfluidics and reduce the product cycle life time [46,47]. Ultimately, the chance of designing innovative and true 3D structures and the material diversity are particularly attractive in the field of microfluidics. In addition to monolithic, single-stage approaches, additive manufacturing enables the design and realization of integrated, modular, or hybrid flow systems to meet user-specific demands and combine several tasks on a small scale [48]. However, the huge potential is also accompanied by great complexity. With this article we provide a further-growing community with a guide to catch up with the state-of-the-art fabrication in microfluidics. The focus is on design, prototyping, fabrication, and post-processing to create proper working multiphase flow systems that are printed using SLA. The approach follows a typical workflow by considering the resin choice, increasing the printer performance, and ultimately post-processing and surface treatment of the printed microchannels. By addressing various challenges and providing a standardized design and prototyping process, we aim to promote the accessibility of microfluidics. Finally, the design methods presented are put into practice using the example of droplet formation with a modular co-flow device and a monolithic flow-focusing device. The co-flow setup is intended for continuous operation with constant fluid flows. With a tapered channel and adaptive positioning of the cannula inside the capillary, it is possible to set different flow regimes with the same device under the same process conditions. For the flow-focusing device, the effects of the considered design options on multiphase flow formation are highlighted. This enables the development of a suitable device in a very short time that covers a wide range of flow regimes depending on the fluid flows.

## 2. Materials and Methods

The following subsections deal with the printer characterization and optimization process, a general device design strategy, and surface treatment protocols to award the

chosen material with the desired properties. In addition to cleaning, this includes treatments to make 3D printable resins optically transparent and either hydrophobic or hydrophilic.

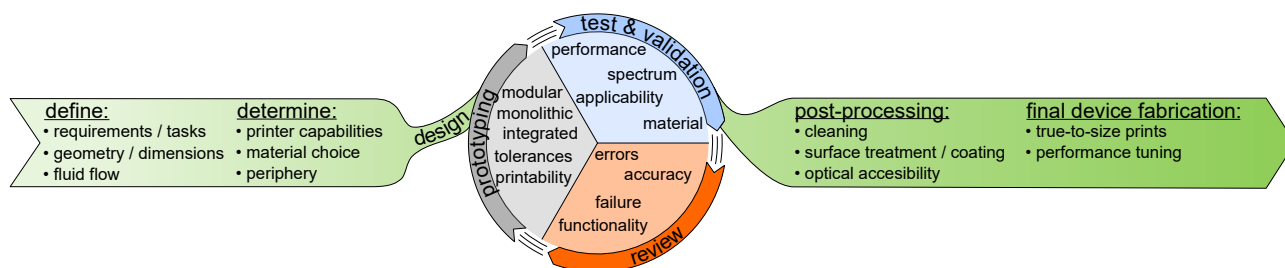
### 2.1. Printer Characterization

Since additive manufacturing revolutionizes the state-of-the-art fabrication of microfluidic devices, it is essential to characterize and optimize the 3D printing process and the post-processing routine to obtain devices that are true to size and feature certain needs. In general, there are two interdependent opportunities to optimize the printing process as such. The first one is to optimize the printer settings that affect the quality and the dimensions of the printed device. This should be the choice if commercially available resins are suitable for the intended application. The other, more complex chance is to tune available resins by blending or develop new resins from scratch that feature the desired properties. For rather complex and demanding devices, both the printer and the resin may be tuned simultaneously to achieve the best results. The blending and formulation process for different resins is well described in the literature, so that the following chapter will focus on tuning the printer at hand to enhance device quality [49–51].

As there are many different printers and printing techniques to fabricate microfluidic devices, it needs to be mentioned that the focus of this contribution is on laser-based SLA printers. The printer that was used for this study is a Formlabs Form 3+ (Formlabs, Somerville, MA, USA) SLA printer, and the optimization was performed exemplarily for a transparent resin that allows for optical analysis (Clear Resin v4, Formlabs, Somerville, MA, USA). The printer is equipped with a 250 mW laser that has a spot size of 85  $\mu\text{m}$ . The lateral resolution in the XY-plane is 25  $\mu\text{m}$ . Consequently, under optimum conditions, positive structures can be printed with a minimum lateral distance of 85  $\mu\text{m}$  at a resolution of 25  $\mu\text{m}$ . The layer height is dependent on the material to be printed and the laser intensity.

### 2.2. Device Design

The development of new microfluidic devices by additive manufacturing requires various design considerations. First, the requirements and necessary performance of the device need to be clarified. Design parameters such as the geometry and the dimensions of the device need to be defined to achieve the desired fluid flow. In addition, the capabilities of the existing printer, the desired material, and the laboratory peripherals must be determined. With this information, the design process starts, where the aim is to develop a first printable CAD model. The design then goes through an iterative process consisting of testing and validation, review, and prototyping to increase the device's quality and performance. Further post-processing that deals with cleaning, surface treatments or coatings, and enhancing optical transparency is needed to enable the device's actual applicability. With all these considerations, the device is ready for final true-to-size fabrication and performance optimization. Figure 1 provides an overview of the development process for additively manufactured microfluidic devices. The process is examined in more detail in the following subchapters.



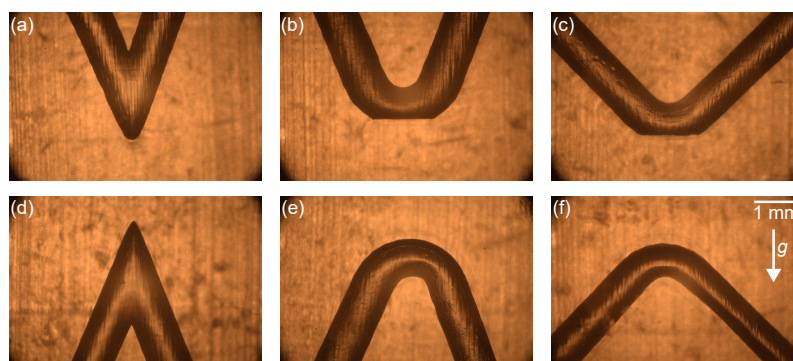
**Figure 1.** This figure shows a guide through the development process of microfluidic devices for multiphase flow applications, starting with the initial idea and needs, the design and rapid prototyping process, and finally the finished product.

### 2.2.1. Design Thinking

At the beginning of each design process for microfluidic devices, the user and the developer need to define its designated features. The main task the device should be able to perform and how this task is performed should be elaborated. Certain geometries and dimensions represent essential design parameters as they affect the flow regime, flow behavior, mixing quality, and residence time of microfluidic devices. With complex tasks and the urgency of innovation comes creativity, and associated to it is the question of whether the desired device is printable. This is even more relevant as additive manufacturing enables the fabrication of true 3D structures, and, hence, the printability in different spatial orientations needs to be considered. Based on the complexity of the device or in the case that several tasks need to be combined, either monolithic, integrated, or modular setups can be beneficial. By determining the printer capabilities and choosing the desired material, it becomes evident which design strategy should be pursued. Depending on whether it is a single-purpose or multi-purpose application, it is essential to evaluate whether the selected material is suitable for use with the desired liquids. The material should therefore be subjected to a durability study, whereby particularly the continuous phase of the multi-phase flow must be evaluated, as it is in constant contact with the material. If there are any issues with the material compatibility but some features of the resin are essential for the application, like optical accessibility or heat resistance, a surface coating might be suitable to make the material compatible. Ultimately, the device must be designed in such a way that fluidic connections can be integrated to ensure the leakage-free supply of fluids and to enable inline analytics.

### 2.2.2. Rapid Prototyping

As a first step, the general printability of the designated prototype needs to be evaluated. The highest possible resolution of the printer at hand should be used, and it is advisable to test different spatial orientations of the device on the build plate, as the printing angle has a great influence on the quality of particularly closed channels, which is emphasized in Figure 2. Internal supporting structures should be avoided as they cannot be removed after printing and would affect the device's performance. Another important part during this stage is to evaluate if the necessary post-processing is applicable to the printed part.



**Figure 2.** Various redirections of channels with an inner diameter of  $d_i = 1$  mm. (a–c) were printed in an orientation that affects the printability of negative structures, and (d–f) were printed after rotation by  $180^\circ$ , resulting in a structure where the printability of channels is not influenced. The direction of gravitational force is indicated.

In the case that the desired design cannot be printed accurately, an iterative prototyping process is necessary to make the prototype producible. The initial design is tested and validated regarding its performance, applicability, and the chosen material. Based on the results, the review phase begins, in which printing errors, printing accuracy, and functionality are taken into account, among other things. For the next prototype, the general

printability, the needed tolerances, and whether a monolithic, modular, or integrated setup is the favorable choice.

Once the printing process provides sufficient results, the device should be tested and evaluated regarding its applicability. If the device does not perform as desired, another iteration process is necessary in order to optimize the post-processing or device design. With regard to multiphase flows in capillaries, these can be leakage, flow disturbances, irregular flow patterns, bad mixing, undesired droplet or slug size, or undesired wetting of the dispersed phase, to name some of the most common. While bad mixing and undesired droplet or slug sizes can be attributed to the dimensions and geometries of the device or to the fluid velocities, flow disturbances, irregular flow patterns, and undesired wetting behavior may be caused by insufficient post-processing.

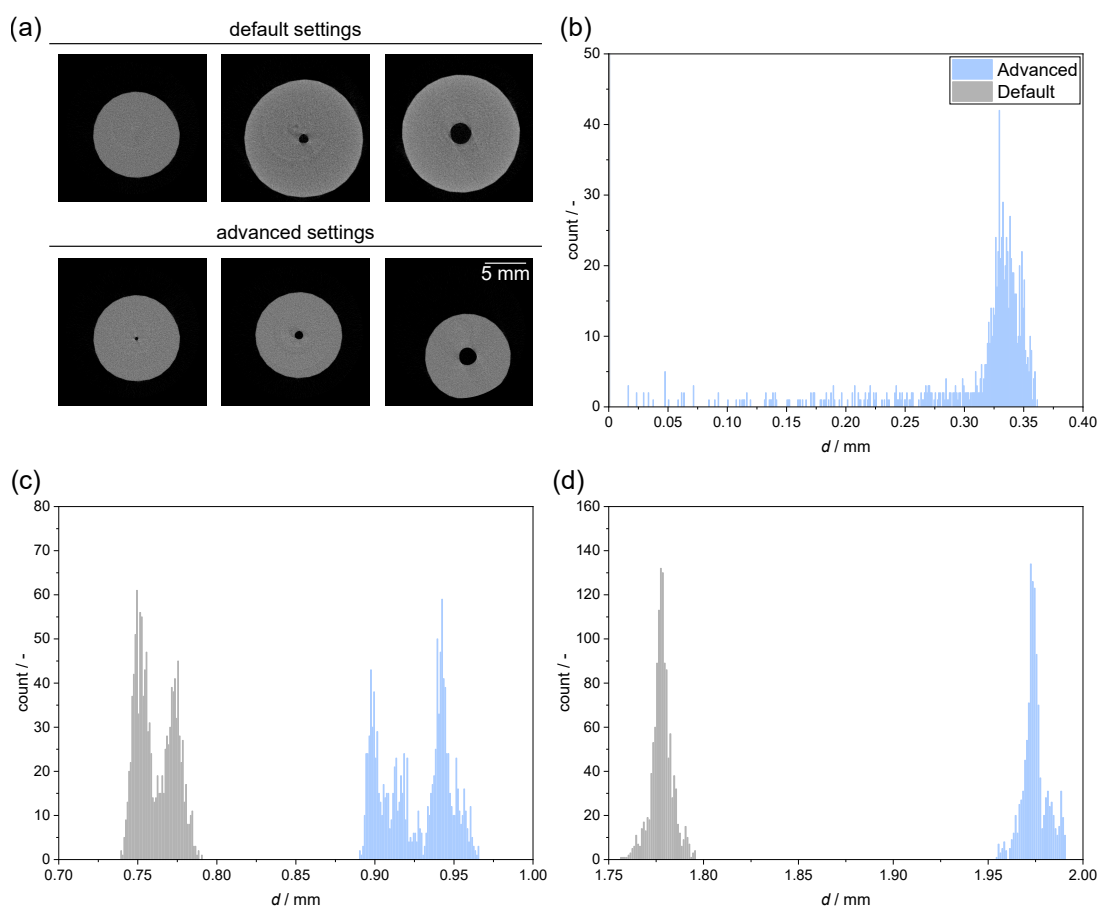
The performance of the device can also be affected by the fact that the dimensions after the printing and post-processing will most likely not be true to size due to swelling or shrinking of the resin or uncured resin sticking to the device because of high capillary forces. Consequently, another important fine-tuning iteration aims at achieving true-to-size fabrication. This can be achieved either by redesigning the device with a certain factor and iteration or by advancing the default parameters of the used printer. This iteration step can be performed either before or after the applicability test. If the printer is intended exclusively for printing microstructures, probably with a large number and fairly complex geometries, it is advisable to change and advance the printer settings. In the case of laser-based printers, such as the one used during this study, the most effective tuning parameters can be seen in Table 1. For other printing techniques, such as light-emitting diode (LED) screens or photon beams, the device quality can be enhanced by tuning similar parameters.

**Table 1.** The tested parameter, their default values, and the advanced values according to this study.

Printing Parameter	Reason to Modify *	Default Value	Advanced Value
Layer thickness	To adjust print speed, surface finish, or Z-axis fine feature performance. Increasing this value can improve print speed. Decreasing this value can improve surface finish or fine feature resolution.	25 $\mu\text{m}$	25 $\mu\text{m}$
X, Y, Z correction factor	To adjust dimensional accuracy of large features (larger than several millimeters) in the X, Y, or Z direction and compensate for the volumetric shrinkage of each material.	1.005; 1.005; 1	1; 1; 1
Perimeter to nominal geometry spacing	To correct for cases where small features (millimeter scale) are undersized or oversized.	−0.05 mm	0 mm
Perimeter fill exposure	To change the surface hardness and surface tackiness of the model. Increase this value to make the print surfaces harder and less tacky.	31 $\text{mJ cm}^{-2}$	20 $\text{mJ cm}^{-2}$
Model fill exposure	To change the green state strength and stiffness of the model. In most cases, higher green strength results in better print success rate, surface finish, and dimensional accuracy.	31 $\text{mJ cm}^{-2}$	20 $\text{mJ cm}^{-2}$
Top surface exposure	To change the surface tackiness or surface hardness of any flat top surfaces on the print.	31 $\text{mJ cm}^{-2}$	20 $\text{mJ cm}^{-2}$
Operating temperature	To adjust the resin temperature that the printer maintains during printing. Higher resin temperatures usually increase resin reactivity and decrease resin viscosity. Increased resin reactivity can impact print speed, dimensional accuracy, and surface finish. Decreased resin viscosity can impact print speed, print success rate, and print quality.	35 $^{\circ}\text{C}$	35 $^{\circ}\text{C}$

\* The descriptions can be found in PreForm software 3.41 for Formlabs printers.

A decrease in layer thickness had no positive effect on the fabrication of microfluidic devices, as a decreased laser penetration depth automatically leads to less strongly cross-linked layers and more printing errors. The reduction in the X and Y correction factors has had a positive effect on the printer accuracy in the scale of microfluidic devices, as the laser spot does not exceed the desired dimensions to counteract any shrinkage. This correction is particularly useful for objects with a rather large volume, where shrinkage has a greater effect. For small applications, especially those with negative structures inside, this parameter has a negative effect, as capillary forces increase and more uncured resin remains entrapped in the channels. The perimeter to nominal geometry spacing determines the distance between the outermost perimeter laser path and the model's nominal boundary. The default negative value causes the laser perimeter to be inset larger than the model's nominal boundary, which results in negative features being smaller and positive features being larger than intended in the CAD file. This effect is counteracted by adjusting this parameter. All other parameters that are varied concern the exposure. As the laser spot has no uniform intensity over its diameter of 85  $\mu\text{m}$ , but features a circular normal distribution, the decrease in this value reduces the laser spot size as the intensity at the marginal areas is too low to harden any resin. A further decrease lower than 20  $\text{mJ cm}^{-2}$ , however, leads to incorrect printing. The performance of the printer's default settings and the advanced settings are emphasized in the histograms in Figure 3. For quantification, the diameters of the capillaries were measured using a micro-computed tomography scanner (Bruker Skyscan 1275, RJI Micro & Analytic GmbH, Karlsdorf-Neuthard, Germany) featuring a resolution of 15  $\mu\text{m}$ . Some exemplary cross-sectional images for different settings and intended diameters are given in Figure 3a. The diameters are evaluated at 500 different positions for each capillary.



**Figure 3.** (a) shows cross-sectional images of the CT scans, that were used for the quantification. The top row represents the default settings and the bottom row the advanced settings for an intended



diameter of 0.5, 1.0, and 2.0 mm (from **left** to **right**). (**b–d**) give the histograms of the diameter distributions for all intended capillary diameters. The histograms of the advanced settings are given in light blue, the histograms of the default settings are given in gray.

The histogram in Figure 3b demonstrates that an intended capillary diameter of  $d_{\text{cap.}} = 0.5$  mm is not realizable with the default printer settings. Even for the advanced settings, it is not possible to come close to the desired diameter as the histogram peaks between 0.31 mm and 0.35 mm. The rather large deviation can be explained by the fact that the material swelling is large in relation to the size of the negative structure. At this level, further adjustments should consider the CAD modeling to improve the print accuracy. For an intended diameter of 1.0 mm, the advanced settings show a better performance than the default settings of the printer, as shown in Figure 3c. The bimodal distributions can be attributed to the instability of the capillaries with increasing distance from the build plate, which leads to a deterioration in print quality in both cases. In similar cases, it is advisable to increase the material thickness to increase the stability. For increasing negative structures, the distribution becomes more narrow, which emphasizes an increased precision of the printer and negligible shrinkage or swelling of the material compared to the capillaries dimensions. Figure 3d demonstrates that the advanced settings outperform the default settings.

### 2.2.3. Periphery Interfaces

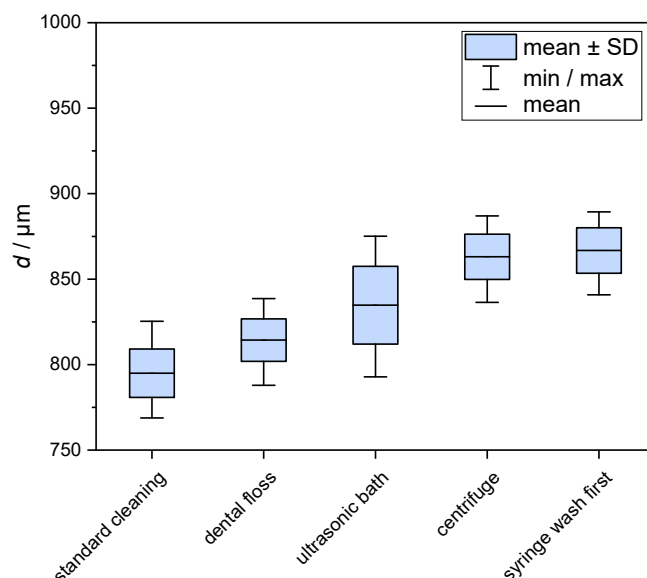
Although microfluidic devices themselves feature small dimensions and are space-saving, the surrounding periphery for fluid supply and drainage and analytical tools is rather macroscopic in most cases. Another benefit of additive manufacturing is that fluidic connections and interfaces to integrate analytics can be customized easily to meet specific needs. Consequently, it is possible to design and print a suitable connection for any type of periphery. This not only promotes the further miniaturization of microfluidics, but also the modular design in particular, as almost unlimited connection options are enabled. When connecting tubes, sensors, or multiple parts of a modular design in series, it is essential to ensure leakage-free connections that come along with tight and precise transitions and only low pressure losses so the fluid flow is not disturbed. The most common types of connectors include threaded connectors, hose nozzles, and bayonet connectors. Each of them is scalable to fit specific demands and a variety of microfluidic devices.

### 2.3. Surface Treatment After Photopolymerization

Since in microfluidic multiphase applications small disturbances or surface irregularities can have a major impact on flow stability and the prevailing flow regime, proper surface cleaning is essential to achieve true-to-scale structures and smooth channels. After the cleaning process, the channel or capillary surface can be treated so that its wetting behavior becomes either hydrophobic or hydrophilic, depending on whether the organic phase or the aqueous phase is intended as the continuous, wetting phase.

#### 2.3.1. Surface Cleaning

After the desired device has been printed, thorough cleaning is required to obtain a print that is as dimensionally accurate as possible. This is particularly necessary for microfluidics with closed channels, as the capillary forces increase as the channel width decreases, causing the uncured resin to stick to the capillary wall and block it. The different cleaning methods are evaluated by comparing the inner diameter of equal channels with an intended diameter of  $d = 1000$   $\mu\text{m}$ , which are cleaned using different cleaning schedules as can be seen in Figure 4. All capillaries were printed orthogonally to the build plate. Thereby the average diameter of the channel is the main characteristic for evaluating the influence of a cleaning method on the print quality. Again, the diameters of the capillaries were measured using micro-computed tomography for this purpose.



**Figure 4.** Diameter distribution of 3D-printed capillaries with an intended diameter of  $d = 1000 \mu\text{m}$  after the application of different cleaning protocols. The boxes give the mean diameter with standard deviation, the whiskers are the minimum and maximum diameters, and the mean diameter is emphasized by a horizontal line.

The standard cleaning schedule consisted of washing the device in the FormWash (Formlabs, Somerville, MA, USA) for 20 min and subsequent flushing with fresh isopropyl alcohol (IPA) (Sigma-Aldrich, St. Louis, MO, USA) in 3 runs with 5 mL each. This cleaning procedure yielded an average diameter of  $785 \mu\text{m}$ . Based on this, it can be stated that every cleaning mechanism causing a greater average diameter has a positive effect on the overall quality of the cleaning schedule. Besides the average diameter, the distribution of the measured diameters holds information about the quality of the cleaning schedule, as a more narrow distribution implies a smoother surface and thereby a more effective cleaning procedure. The possible cleaning steps considered are the washing in an ultrasonic bath (Elmasonic S30 H, Elmasonic, Singen, Germany), mechanical cleaning with padded dental floss (Oral-B, Northwich, Cheshire, UK) and a spring steel wire with a thickness of  $500 \mu\text{m}$ , and the application of centrifugal forces via a self-made attachment for drilling machines.

The mechanical cleaning results in an average diameter of  $823 \mu\text{m}$  and has not shown a recognizable effect on the surface roughness as the standard deviation is still low with  $10.0 \mu\text{m}$ . The energy input of the ultrasonic bath into the liquid results in an increased solubility of the residue resin in the IPA due to convective mass transfer even inside closed channels, resulting in an average diameter of  $846 \mu\text{m}$ . However, the standard deviation is the highest when cleaning in an ultrasonic bath, which is due to the concentration gradients of the IPA along the capillary axis. The greatest influence on the cleaning quality has the usage of centrifugal force with an average diameter of  $870 \mu\text{m}$ . This increase can be explained by the fact that the rinsing with IPA only affects the surface of the resin, whereas the centrifugal force acts on the whole mass of the uncured resin. Besides the most accurate average diameter, this cleaning method also provides the narrowest distribution with a standard deviation of  $8.9 \mu\text{m}$ , which implies a smooth surface structure. Rinsing with a syringe instead of washing the device in IPA first has no significant effect on cleaning if the next steps are performed in the same way. For closed channels that are smaller than  $500 \mu\text{m}$  or are of complex channel arrangement, the application of pressurized air has been proven to be an efficient replacement for the mechanical cleaning. The optimized cleaning protocol is as follows:

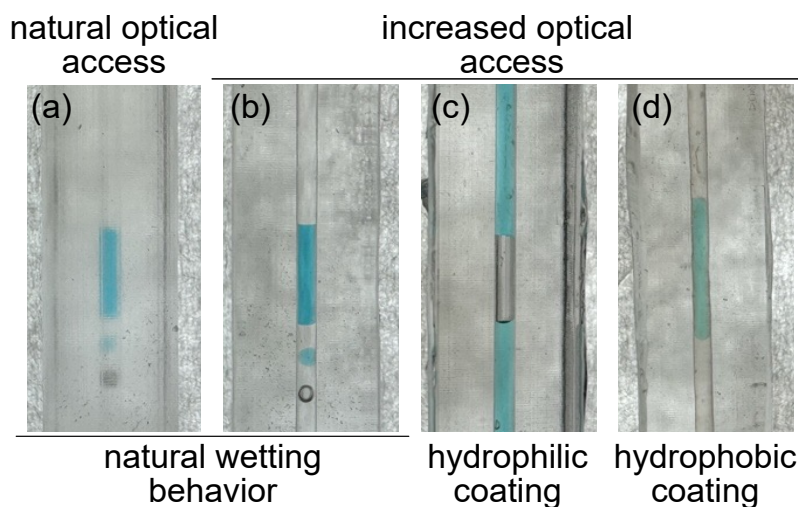
- Cleaning the outer surface of the printed device by rinsing it in a tank of IPA for 20 min.
- Application of an ultrasonic bath at 37 kHz, 320 W, and  $30^\circ\text{C}$  for 10 min.

- Flushing the channels 3 times with a syringe, which is filled with 5 mL of fresh IPA, removing most of the resin from the inside of the channels.
- Placing the parts inside a centrifuge to remove the resin, which could not be affected by the previous flushing process, with centrifugal force.
- Removing the IPA and the least amount of resin using a spring steel wire and dental floss, which not only removes the resin solved in the IPA, but also scrubs the inside walls of the channels and clears it from resin that sticks to the surfaces.
- Flushing the channels again as explained in step 3.
- Drying the device with pressurized air before final UV radiation.

### 2.3.2. Optical Accessibility

As imaging is one major analysis tool in microfluidic applications, optical accessibility is essential to evaluate the performance of many devices. For optical accessibility, it is evident to choose a transparent resin for fabrication. Due to the layer-by-layer printing process, however, optical accessibility can be limited, as individual layers interfere with the beam path and impair the evaluation options. The optical transparency of resins can be improved by using various fast auxiliaries or longer-lasting coatings.

The application of adhesive tape or clear coat is a quick aid to improve visual accessibility. A single-step procedure for a robust and long-lasting transparency with a glass-like surface is to apply a thin film of the same resin to the device. A glass object, such as a cover glass or petri dish, is then placed on top of the applied resin to create a flat layer. The device is then radiated with UV light to polymerize the resin film. A non-treated surface and a surface after applying a thin resin film can be seen in Figure 5a–b.



**Figure 5.** (a) shows a 3D-printed channel with an inner diameter of  $d_i = 1$  mm with the natural optical access and the natural wetting behavior of the resin. (b–d) show a channel with increased optical accessibility with (b) natural wetting behavior, (c) wetting after hydrophobic coating, and (d) wetting after hydrophilic coating. The blue liquid is DI water with ink, and the transparent liquid is silicon oil.

### 2.3.3. Hydrophobic Coating

In multiphase flows, the fluid that is desired to be the continuous phase must wet the channel wall, while the dispersed phase should have a rather high contact angle to enable stable segmented flow regimes. However, it occasionally happens that the favored resin for a particular application is not of hydrophilic or hydrophobic nature and limits the applicability as no reliable multiphase flow can be established. In that case, it is possible to treat the surface with certain protocols to give the capillaries the desired property regarding the wetting behavior of the fluids involved. Although for open-channel structures the surface coating can be achieved with well-established plasma treatments, closed channels, especially with more complex geometries, need an alternative method. A suitable method

is to perform a treatment with a liquid phase that is filled into the channel. The contact angle of water with the resin surface can be increased by liquid-phase silanization, making the surface hydrophobic, as reported by [52]. In two previous studies that deal with the 3D evaluation of droplet formation [53] and continuous liquid–liquid phase separation in 3D-printed devices [54], we applied the protocol to further UV-sensitive resins and extended the feasibility of the treatment. During the treatment (tridecafluoro-1,1,2,2-tetrahydrooctyl-) trichlorosilane is covalently bonded to the resin surface as its keto groups are oxidized during the process. The effect of the treatment is shown in Figure 5c. The protocol for the hydrophobic coating is as follows:

- Fill the capillary or channel with a solution of 10 vol.-% of the silane (Thermoscientific, Kandel, Germany) in FC-40 (Sigma-Aldrich, St. Louis, MO, USA) for 30 min at room temperature. Ensure that all parts that get in contact with the liquids during application are covered during the treatment.
- Rinse the capillary or channel with a 95 vol.-% ethanol (Sigma-Aldrich, St. Louis, MO, USA) in DI water solution to remove non reacted silane.
- Dry the coated device with nitrogen.

#### 2.3.4. Hydrophilic Coating

Vice versa, in the case that the aqueous phase is desired to be the wetting phase, a different treatment is necessary to establish a hydrophilic coating of the resin. A liquid-phase coating is also desired here to handle closed channels [55]. The effect of the treatment is emphasized in Figure 5d. The protocol for hydrophilic surface coating is as follows:

- Dissolve 2 mol L<sup>−1</sup> metacrylic acid (Sigma-Aldrich, St. Louis, MO, USA) and 0.004 mol L<sup>−1</sup> bisphenol (Sigma-Aldrich, St. Louis, MO, USA) in a 20% ethanol (Sigma-Aldrich, St. Louis, MO, USA)/DI water mixture.
- Fill the solution into the capillary or channel and expose it to UV light at 405 nm for 6 min.
- Rinse capillary or channel with DI water after the reaction.

#### 2.4. Final Device Fabrication and Experimental Setup

The final devices, the design and prototyping of which are discussed in this article, were manufactured using the following process. They were made of Formlabs Clear resin v4 on a Formlabs Form 3+ printer. The selected layer thickness orthogonal to the printing platform was 25 µm. The advanced printing settings to achieve true-to-size prints for the used printer are listed in Table 1. After the printing process, the devices were cleaned according to the previously elaborated cleaning protocol. After that, the liquid-phase hydrophobic coating was applied to the channels. Optical accessibility was increased by adding a thin resin film to the outer surface of the devices. The chosen periphery was 1/4"-28 Unified National Fine Thread Series (UNF) IDEX fittings (IDEX HS, Wertheim, Germany) to connect fluoroethylene propylene (FEP) laboratory tubing with an inner diameter of 1.6 mm and an outer diameter of 3.2 mm. For fluid supply, two syringe pumps (VIT-FIT, LAMBDA Laborgeräte, Zurich, Switzerland) were used. Due to the hydrophobic coating, PDMS (PDMS-1cSt, ELBESIL-Öle B, L. Böwig GmbH, Hofheim, Germany) was used as the wetting, continuous phase, and DI water was used as the dispersed phase. To enhance the contrast between both phases, blue ink (4001, Pelikan Holding AG, Hanover, Germany) was added to the DI water. Volumetric flow rates are in the range of 0.05–5 mL min<sup>−1</sup>.

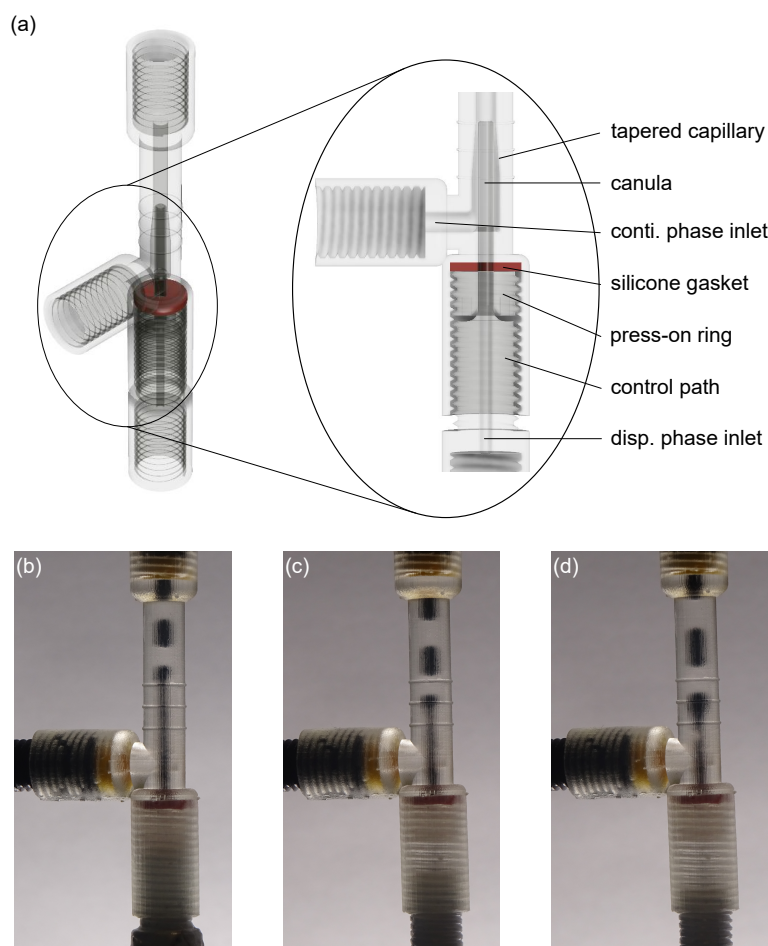
### 3. Results

The most important opportunity to control the performance of multiphase flows is during the emergence of the dispersed phase. There are several methods to control the droplet size as the main influential parameter of flow chemistry processes, as it determines the ratio of the interfacial area and its volume. In this part of the article, a monolithic

approach and a modular approach are presented and discussed regarding their applicability in microfluidic multiphase flows.

### 3.1. Adjustable Co-Flow Setup

The adjustable co-flow device is a modular setup that consists essentially of a capillary and a cannula that are both 3D-printed. The setup and a close-up can be seen in Figure 6a. Right at the t-junction of the co-flow setup, the capillary features a diameter of  $d_{\text{cap},i} = 2.5$  mm that tapers over a distance of 5 mm until a diameter of  $d_{\text{cap},i} = 1.8$  mm is reached. A thread is used to adjust how far the tip of the cannula, where the droplet formation happens, protrudes into the capillary. As the geometry and dimensions of the capillary have a significant influence on droplet formation, this design can be used to control the entire process without the need to change any process equipment or fluid flows. The cannula has an inner diameter of  $d_{\text{can},i} = 1$  mm and an outer diameter of  $d_{\text{can},o} = 1.4$  mm. The length of the part of the cannula that penetrates the capillary can be varied from  $l_{\text{can}} = 4.5$ –9.5 mm to match the tapered distance of the capillary. To ensure a leakage-free process, a silicon gasket is pressed onto the channel, which is used to insert the cannula into the capillary and is punctuated by the cannula. A 3D-printed press-on ring that features a thread and a hole for the cannula is used for this purpose. The thread behind determines the stroke distance and hence the control path of the cannula. The design and dimensions of the device are given in Appendix A.



**Figure 6.** (a) shows an adjustable co-flow setup and a close-up of the droplet formation area. The adjustment is made by varying the distance by which the cannula protrudes into the capillary. In the tapered section, the diameter of the capillary is reduced from 2.5 mm to 1.8 mm over a distance of 5 mm. (b–d) show an emerging and a detached droplet for different cannula positions and capillary diameters at  $\dot{V}_{\text{conti.}} = 0.25 \text{ mL min}^{-1}$  and  $\dot{V}_{\text{disp.}} = 0.25 \text{ mL min}^{-1}$ .

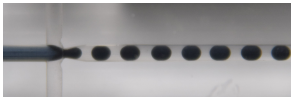
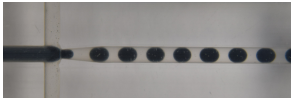
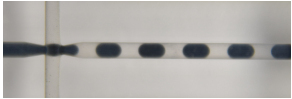

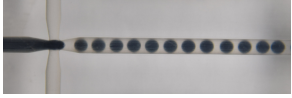


At rather low flow rates as present for the leaking and squeezing regime, the dimensions of the emerging droplets depend on the diameter of the capillary. During the filling stage, the droplet grows simultaneously in axial and radial directions until its diameter comes close to the capillary diameter. The subsequent necking stage is characterized by droplet growth in the axial direction and finally the pinch-off of the droplet. With a tapered channel, the fluid velocity of the continuous phase at the cannula tip and hence the shear forces acting on the emerging droplet are manipulated, so that the size of the droplet can be controlled. For an increasing capillary diameter, larger droplets are formed, as can be seen in Figure 6b–d at constant volumetric flow rates of  $\dot{V}_{\text{conti.}} = 0.25 \text{ mL min}^{-1}$  and  $\dot{V}_{\text{disp.}} = 0.25 \text{ mL min}^{-1}$ . As a consequence, the droplet formation frequency, the droplet size, and the distance between two droplets can be adjusted while keeping the throughput and the volumetric flow rates of the fluids involved constant. The ability to manipulate the droplet size in such a way is particularly important in processes where the ratio between the surface area and the volume of the droplets is crucial.

### 3.2. Flow-Focusing Device

A flow-focusing device is the preferable choice when a monolithic setup should cover a wide range of different droplet and slug sizes or when a high formation frequency of the dispersed phase is required. Table 2 provides a basis for which design parameters should be considered during prototyping and what influence they have on the dominant flow regime. It is worth noting that all monolithic flow-focusing devices were printed with all channels aligned at  $45^\circ$  to the build plate to achieve the best printing results. The considered design parameters are the diameter of the inlet channels  $d_{i, \text{conti.}}$  and  $d_{i, \text{disp.}}$  and the opening angle of the orifice  $\theta_{\text{orifice}}$ , while the orifice diameter was kept constant at  $d_{\text{orifice}} = 1.0 \text{ mm}$  and the diameter outlet was kept constant at  $d_o = 1.6 \text{ mm}$ . The volumetric flow rates of both phases were  $\dot{V}_{\text{conti.}} = \dot{V}_{\text{disp.}} = 0.25 \text{ mL min}^{-1}$  for all experiments.

**Table 2.** History of the prototyping for the flow-focusing setup with a circular cross-section and the effect on the droplet size for varied design parameters at constant volumetric flow rates  $\dot{V}_{\text{conti.}} = 0.25 \text{ mL min}^{-1}$  and  $\dot{V}_{\text{disp.}} = 0.25 \text{ mL min}^{-1}$ . The orifice diameter was kept constant at  $d_{\text{orifice}} = 1.0 \text{ mm}$ ;

Prototype	Two-Phase Flow	Changelog *	Flow Regime
P1.0		$d_{i, \text{conti.}} = d_{i, \text{disp.}} = 1.6 \text{ mm};$ $\theta_{\text{orifice}} = 10^\circ$	stable and uniform slug flow
P1.1		$\theta_{\text{orifice}} = 20^\circ$	stable and uniform slug flow with slightly smaller slugs; high slug formation frequency
P1.2		$d_{i, \text{disp.}} = 1.0 \text{ mm}$	stable and uniform slug flow with larger slugs; low slug formation frequency
P1.3		$d_{i, \text{conti.}} = 1.0 \text{ mm}$	droplet flow; high drop formation frequency
P1.4		$d_{i, \text{disp.}} = d_{i, \text{conti.}} = 1.0 \text{ mm}$	droplet flow; high drop formation frequency

\* Compared to prototype P1.0.

The prototype P1.0 is considered the benchmark from which the influences of the various design parameters are evaluated. At the given volumetric flow rates, stable and uniform slug flow is present for P1.0. When increasing the opening angle of the orifice from  $\theta_{\text{orifice}} = 10^\circ$  to  $\theta_{\text{orifice}} = 20^\circ$  (P1.1), stable slug flow is achieved with only slightly smaller slugs than for P1.0. As the dispersed phase protrudes into the main channel during slug formation, the capillary dimensions determine the slug size, as described for the adjustable co-flow setup. The larger the opening angle, the longer the distance required to reach the main channel dimension. At the same fluid velocity at the orifice, the dispersed phase protrudes the same distance into the main channel. Due to the smaller diameter at the point where the dispersed phase is sheared off, the slugs formed are smaller than with P1.0.

For P1.2 the diameter of the inlet channel for the dispersed phase was changed from  $d_{i, \text{disp.}} = 1.6 \text{ mm}$  to  $d_{i, \text{disp.}} = 1.0 \text{ mm}$ , which results in an acceleration of the dispersed phase. Consequently, larger slugs form at the orifice, as the dispersed phase passes through with a higher velocity than the continuous one that shears off the slug. Accordingly, the formation frequency decreases and the distance between slugs increases if the volumetric flow rates remain the same.

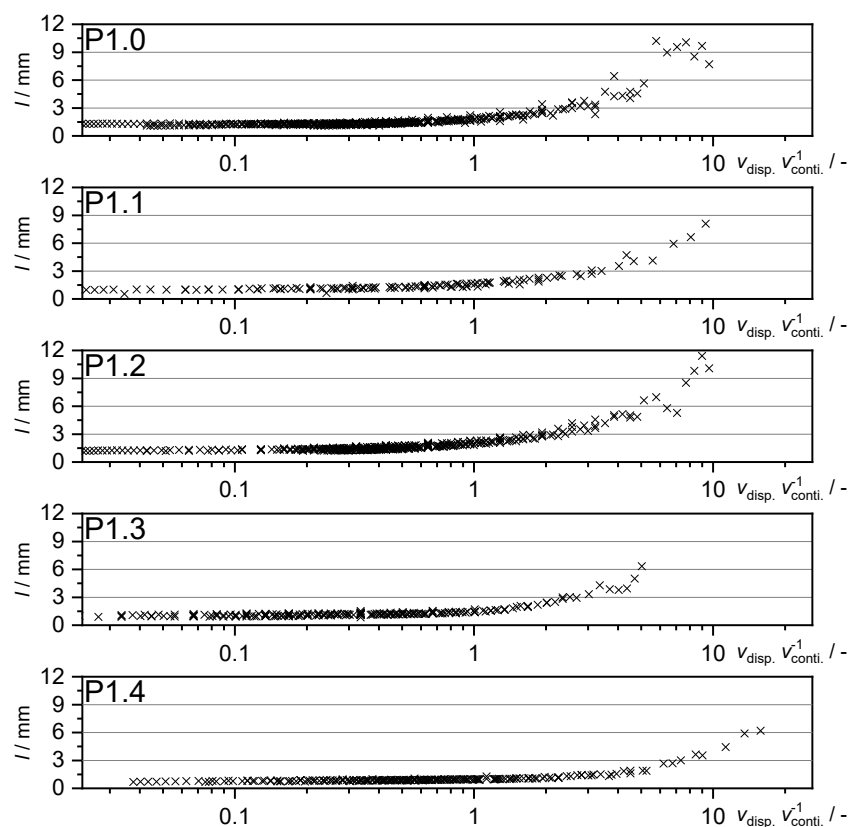
Vice versa, in case that the diameter of the inlet channels of the continuous phase are decreased from  $d_{i, \text{conti.}} = 1.6 \text{ mm}$  to  $d_{i, \text{conti.}} = 1.0 \text{ mm}$ , the predominant flow regime changes from slug flow to droplet flow. Due to the increased velocity of the continuous phase the dispersed phase is sheared off faster after passing through the orifice and the small volumes lead to stable droplet flow. Consequently, the frequency of droplet formation is higher and the distance between the droplets is smaller than with the previous prototypes.

For P1.4 both, the diameters of the inlet channels for the dispersed phase and for the continuous phase were changed from  $d_{i, \text{conti.}} = d_{i, \text{disp.}} = 1.6 \text{ mm}$  to  $d_{i, \text{conti.}} = d_{i, \text{disp.}} = 1.0 \text{ mm}$ . Accordingly, the velocity ratio of both phases is the same as for P1.0, and one would expect that the same flow regime should be present in that case. However, it becomes evident that P1.4 promotes the same flow regime as P1.3 for constant volumetric flow rates, which suggests that the velocity of the continuous phase is the dominant factor influencing droplet formation and has the greater influence on the present flow regime.

In addition to the design parameters presented in this paper, changing the orifice diameter or the contact angle of the two phases involved could be considered as other options to control the fluid flow. Ultimately, it can be said that the design and prototyping process for flow-focusing devices is complex, as there are many parameters that have to be evaluated. However, following the prototyping, a sufficient device that has a customized bandwidth to effectively control the droplet size based on the involved fluid flows is obtained.

These geometrical influences are emphasized in Figure 7, where for each prototype the droplet, slug length  $l$  is plotted over the phase velocity ratio  $v_{\text{disp.}} v_{\text{conti.}}^{-1}$ . With an increasing phase velocity ratio, a transition from droplet flow to slug flow can be observed. While there is only a small effect of the orifice opening angle, the steeper slope for P1.2 shows that a smaller inlet channel of the dispersed phase promotes slug formation. The exact opposite effect can be seen for P1.3 and P1.4, where the slope of the graph is much flatter and droplets are generated over a wide range of phase velocity ratios.

The typical time during the prototyping process for the flow-focusing device takes 1 d for the first design and the printing process; the cleaning and the surface treatments take another 3–4 h. The time to test and evaluate the performance by image analysis depends on the application the user is exactly looking for, but 1–2 d should be expected. After that period, the review and redesign start before entering the same cycle again. It helps to design and print several devices concerning the same design parameter at once to make even faster progress.



**Figure 7.** Droplet and slug length  $l$  plotted over the phase velocity ratio  $v_{\text{disp}} \cdot v_{\text{conti}}^{-1}$ . Graphs are labeled for P1.0–P1.4.

#### 4. Conclusions

The field of microfluidics has come a long way since its inception, driven by advancements in manufacturing techniques and the visionary contributions, in particular by Prof. G. M. Whitesides and his group. The integration of additive manufacturing has opened new frontiers in the design and fabrication of microfluidic systems, offering increased flexibility, true 3D structures, and rapid prototyping. As rapid prototyping and design thinking continue to shape the state of the art in microfluidic fabrication, the potential for innovation and application in this field remains at a high level. By embracing these modern fabrication techniques and approaches, researchers continue to improve microfluidic technology, leading to new discoveries and solutions that address some of the most urgent challenges in science and medicine.

With this contribution we aim at helping researchers, especially those new to the field, to catch up to the state-of-the-art fabrication of microfluidics and at promoting accessible and affordable fabrication methods to a steadily growing microfluidics community. The article addresses the design and prototyping process of additive manufactured microfluidics, their actual fabrication, and some necessary material treatments to make the devices suitable for the application in multiphase flows. To achieve true-to-size devices, a parameter tuning of commercially available laser-based SLA printers was presented. It was determined that the X and Y correction factors, the perimeter to nominal geometry spacing, and the exposure had the greatest influence for the present printer. The orientation of the channels on the build plate during the printing process should ideally be 90°. A suitable cleaning schedule was presented, showing the effects of mechanical cleaning, cleaning with an ultrasonic bath, and cleaning with liquid flow. In order to make SLA-printed microfluidics applicable for multiphase flows, a hydrophilic and hydrophobic surface coating as well as a method to increase optical transparency were presented. Ultimately, two design ideas were fabricated, and the impact of relevant design features regarding their influence on droplet formation in liquid-liquid flows

was evaluated. The modular co-flow setup has been proven to be a simple but effective method to control the droplet dimensions and droplet spacing for constant fluid flow. As the droplet or slug size depends on the dimensions of the capillary, a wider capillary leads to larger segments of the dispersed phase and more space in between two ascending droplets or slugs. Vice versa, a smaller capillary diameter leads to smaller segments with a higher formation frequency and less spacing. The tapered channel enables infinitely adjustable droplet and slug sizes at a given flow rate. For the monolithic flow-focusing device, it became apparent that the fluid velocities have the greatest influence on droplet or slug size and the formation frequency, whereas the velocity of the continuous phase dominates. The velocity of both phases can be varied by the diameter of the inlet channel if the flow rates are to be kept constant. To cover a wide range of different droplet and slug sizes, the inlet for the dispersed phase is the most important design parameter and should be smaller than the inlet channel for the continuous phase. This accelerates the dispersed phase, resulting in stable slug flow formation. This was determined in an iterative design and prototyping process in a short time. The finished devices cannot be adjusted during a running process; the droplet size is controlled via the volumetric flow rates of the fluids involved.

**Author Contributions:** Conceptualization, B.O.; methodology, B.O., R.F., T.P., P.T.; software, B.O., R.F.; validation, B.O., and N.K.; investigation, B.O., R.F., T.P., P.T.; data curation, B.O.; writing—original draft preparation, B.O.; writing—review and editing, N.K.; visualization, B.O.; supervision, N.K.; funding acquisition, N.K. All authors have read and agreed to the published version of the manuscript.

**Funding:** The Bruker Skyscan 1275  $\mu$ -CT scanner that was used for this research was funded by the German Research Foundation (DFG, grant number INST 212/397-1).

**Data Availability Statement:** The original contributions presented in the study are included in the article, further inquiries can be directed to the corresponding author/s.

**Acknowledgments:** The authors thank RJL Micro & Analytic, Karlsdorf-Neuthard, Germany, and C. Schrömgies (Laboratory of Equipment Design, TU Dortmund University, Germany) for technical support and advice. B.O. thanks the networking program Sustainable Chemical Synthesis 2.0 (SusChemSys 2.0) for the support and valuable discussions across disciplines.

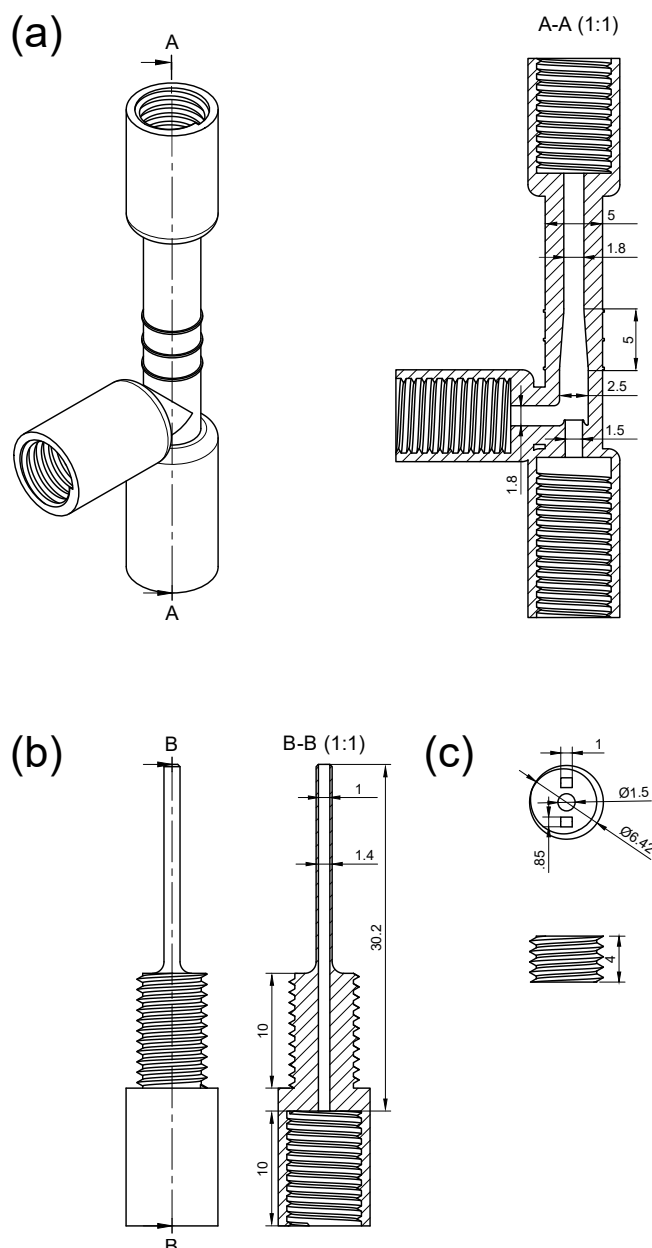
**Conflicts of Interest:** The authors declare no conflicts of interest.

## Abbreviations

The following abbreviations are used in this manuscript:

CAD	computer-aided design
DLP	digital light processing
FEP	fluoroethylene propylene
FFF	fused filament fabrication
IPA	isopropyl alcohol
LOC	lab-on-a-chip
MEMS	micro-electromechanical systems
PDMS	polydimethylsiloxane
SLA	stereolithography
UNF	Unified National Fine Thread Series
$\mu$ TAS	micro total chemical analysis systems

## Appendix A



**Figure A1.** Technical drawings and dimensions of the modular co-flow device. (a) shows the tapered capillary with the T-junction; (b) shows the canula that is inserted into the capillary; and (c) shows the press-on ring for the silicone gasket, as shown in Figure 6.

## References

1. Hansen, C. Microfluidics in structural biology: Smaller, faster... better. *Curr. Opin. Struct. Biol.* **2003**, *13*, 538–544. [[CrossRef](#)] [[PubMed](#)]
2. Theberge, A.B.; Courtois, F.; Schaerli, Y.; Fischlechner, M.; Abell, C.; Hollfelder, F.; Huck, W.T.S. Microdroplets in Microfluidics: An Evolving Platform for Discoveries in Chemistry and Biology. *Angew. Chem. Int. Ed.* **2010**, *49*, 5846–5868. [[CrossRef](#)] [[PubMed](#)]
3. Chen, J.; Chen, D.; Xie, Y.; Yuan, T.; Chen, X. Progress of Microfluidics for Biology and Medicine. *Nano-Micro Lett.* **2013**, *5*, 66–80. [[CrossRef](#)]
4. Song, P.; Hu, R.; Tng, D.J.H.; Yong, K.T. Moving towards individualized medicine with microfluidics technology. *RSC Adv.* **2014**, *4*, 11499. [[CrossRef](#)]
5. Whitesides, G.M. The origins and the future of microfluidics. *Nature* **2006**, *442*, 368–373. [[CrossRef](#)]
6. Ho, C.M.; Tai, Y.C. Micro-Electro-Mechanical-Systems (MEMS) and Fluid Flows. *Annu. Rev. Fluid Mech.* **1998**, *30*, 579–612. [[CrossRef](#)]



7. Tabeling, P. *Introduction to Microfluidics*; Includes Bibliographical References and Index; Oxford University Press: Oxford, UK, 2023.
8. Sun, J.; Warden, A.R.; Ding, X. Recent advances in microfluidics for drug screening. *Biomicrofluidics* **2019**, *13*, 061503. [[CrossRef](#)]
9. Whitesides, G.M.; Stroock, A.D. Flexible Methods for Microfluidics. *Phys. Today* **2001**, *54*, 42–48. [[CrossRef](#)]
10. Dinter, R.; Willems, S.; Hachem, M.; Streltsova, Y.; Brunschweiler, A.; Kockmann, N. Development of a two-phase flow reaction system for DNA-encoded amide coupling. *React. Chem. Eng.* **2023**, *8*, 1334–1340. [[CrossRef](#)]
11. Bobers, J.; Škopić, M.K.; Dinter, R.; Sakthithasan, P.; Neukirch, L.; Gramse, C.; Weberskirch, R.; Brunschweiler, A.; Kockmann, N. Design of an Automated Reagent-Dispensing System for Reaction Screening and Validation with DNA-Tagged Substrates. *ACS Comb. Sci.* **2020**, *22*, 101–108. [[CrossRef](#)]
12. Figeys, D.; Pinto, D. Lab-on-a-chip: A revolution in biological and medical sciences. *Anal. Chem.* **2000**, *72*, 330A–335A. [[CrossRef](#)] [[PubMed](#)]
13. De Stefano, P.; Bianchi, E.; Dubini, G. The impact of microfluidics in high-throughput drug-screening applications. *Biomicrofluidics* **2022**, *16*, 031501. [[CrossRef](#)] [[PubMed](#)]
14. Jankowski, P.; Kutaszewicz, R.; Ogończyk, D.; Garstecki, P. A microfluidic platform for screening and optimization of organic reactions in droplets. *J. Flow Chem.* **2019**, *10*, 397–408. [[CrossRef](#)]
15. Bobers, J.; Grün, J.; Höving, S.; Pyka, T.; Kockmann, N. Two-Phase Flow in a Coiled Flow Inverter: Process Development from Batch to Continuous Flow. *Org. Process Res. Dev.* **2020**, *24*, 2094–2104. [[CrossRef](#)]
16. Ding, Y.; Howes, P.D.; deMello, A.J. Recent Advances in Droplet Microfluidics. *Anal. Chem.* **2019**, *92*, 132–149. [[CrossRef](#)]
17. Moragues, T.; Arguijo, D.; Beneyton, T.; Modavi, C.; Simutis, K.; Abate, A.R.; Baret, J.C.; deMello, A.J.; Densmore, D.; Griffiths, A.D. Droplet-based microfluidics. *Nat. Rev. Methods Prim.* **2023**, *3*, 32. [[CrossRef](#)]
18. Garstecki, P.; Fuerstman, M.; Stone, H.; Whitesides, G. Formation of droplets and bubbles in a microfluidic T-junction—Scaling and mechanism of break-up. *Lab Chip* **2006**, *6*, 437. [[CrossRef](#)]
19. Battat, S.; Weitz, D.A.; Whitesides, G.M. Nonlinear Phenomena in Microfluidics. *Chem. Rev.* **2022**, *122*, 6921–6937. [[CrossRef](#)] [[PubMed](#)]
20. Schuler, J.; Neuendorf, L.M.; Petersen, K.; Kockmann, N. Micro-computed tomography for the 3D time-resolved investigation of monodisperse droplet generation in a co-flow setup. *AIChE J.* **2020**, *67*, e17111. [[CrossRef](#)]
21. Mashaghi, S.; Abbaspourrad, A.; Weitz, D.A.; van Oijen, A.M. Droplet microfluidics: A tool for biology, chemistry and nanotechnology. *TrAC Trends Anal. Chem.* **2016**, *82*, 118–125. [[CrossRef](#)]
22. Sackmann, E.K.; Fulton, A.L.; Beebe, D.J. The present and future role of microfluidics in biomedical research. *Nature* **2014**, *507*, 181–189. [[CrossRef](#)] [[PubMed](#)]
23. Guo, M.T.; Rotem, A.; Heyman, J.A.; Weitz, D.A. Droplet microfluidics for high-throughput biological assays. *Lab Chip* **2012**, *12*, 2146. [[CrossRef](#)] [[PubMed](#)]
24. He, Y.; Wu, Y.; Fu, J.; Gao, Q.; Qiu, J. Developments of 3D Printing Microfluidics and Applications in Chemistry and Biology: A Review. *Electroanalysis* **2016**, *28*, 1658–1678. [[CrossRef](#)]
25. Ren, K.; Zhou, J.; Wu, H. Materials for Microfluidic Chip Fabrication. *Acc. Chem. Res.* **2013**, *46*, 2396–2406. [[CrossRef](#)] [[PubMed](#)]
26. Nge, P.N.; Rogers, C.I.; Woolley, A.T. Advances in Microfluidic Materials, Functions, Integration, and Applications. *Chem. Rev.* **2013**, *113*, 2550–2583. [[CrossRef](#)]
27. Nielsen, A.V.; Beauchamp, M.J.; Nordin, G.P.; Woolley, A.T. 3D Printed Microfluidics. *Annu. Rev. Anal. Chem.* **2020**, *13*, 45–65. [[CrossRef](#)]
28. Brittain, S.; Paul, K.; Zhao, X.M.; Whitesides, G. Soft lithography and microfabrication. *Phys. World* **1998**, *11*, 31–37. [[CrossRef](#)]
29. Duffy, D.C.; McDonald, J.C.; Schueller, O.J.A.; Whitesides, G.M. Rapid Prototyping of Microfluidic Systems in Poly(dimethylsiloxane). *Anal. Chem.* **1998**, *70*, 4974–4984. [[CrossRef](#)]
30. McDonald, J.C.; Duffy, D.C.; Anderson, J.R.; Chiu, D.T.; Wu, H.; Schueller, O.J.A.; Whitesides, G.M. Fabrication of microfluidic systems in poly(dimethylsiloxane). *Electrophoresis* **2000**, *21*, 27–40. [[CrossRef](#)]
31. Sia, S.K.; Whitesides, G.M. Microfluidic devices fabricated in Poly(dimethylsiloxane) for biological studies. *Electrophoresis* **2003**, *24*, 3563–3576. [[CrossRef](#)]
32. Ng, J.M.K.; Gitlin, I.; Stroock, A.D.; Whitesides, G.M. Components for integrated poly(dimethylsiloxane) microfluidic systems. *Electrophoresis* **2002**, *23*, 3461–3473. [[CrossRef](#)] [[PubMed](#)]
33. Anderson, J.R.; Chiu, D.T.; Jackman, R.J.; Cherniavskaya, O.; McDonald, J.C.; Wu, H.; Whitesides, S.H.; Whitesides, G.M. Fabrication of Topologically Complex Three-Dimensional Microfluidic Systems in PDMS by Rapid Prototyping. *Anal. Chem.* **2000**, *72*, 3158–3164. [[CrossRef](#)] [[PubMed](#)]
34. Chiu, D.T.; Jeon, N.L.; Huang, S.; Kane, R.S.; Wargo, C.J.; Choi, I.S.; Ingber, D.E.; Whitesides, G.M. Patterned deposition of cells and proteins onto surfaces by using three-dimensional microfluidic systems. *Proc. Natl. Acad. Sci. USA* **2000**, *97*, 2408–2413. [[CrossRef](#)] [[PubMed](#)]
35. McDonald, J.C.; Chabinyc, M.L.; Metallo, S.J.; Anderson, J.R.; Stroock, A.D.; Whitesides, G.M. Prototyping of Microfluidic Devices in Poly(dimethylsiloxane) Using Solid-Object Printing. *Anal. Chem.* **2002**, *74*, 1537–1545. [[CrossRef](#)]
36. Bhattacharjee, N.; Urrios, A.; Kang, S.; Folch, A. The upcoming 3D-printing revolution in microfluidics. *Lab Chip* **2016**, *16*, 1720–1742. [[CrossRef](#)]

37. Au, A.K.; Huynh, W.; Horowitz, L.F.; Folch, A. 3D-Printed Microfluidics. *Angew. Chem. Int. Ed.* **2016**, *55*, 3862–3881. [[CrossRef](#)] [[PubMed](#)]
38. Gelhausen, M.G.; Feuerbach, T.; Schubert, A.; Agar, D.W. 3D Printing for Chemical Process Laboratories I: Materials and Connection Principles. *Chem. Eng. Technol.* **2018**, *41*, 618–627. [[CrossRef](#)]
39. Musgrove, H.; Catterton, M.; Pompano, R. Applied tutorial for the design and fabrication of biomicrofluidic devices by resin 3D printing. *Anal. Chim. Acta* **2022**, *1209*, 339842. [[CrossRef](#)]
40. Gyimah, N.; Scheler, O.; Rang, T.; Pardy, T. Can 3D Printing Bring Droplet Microfluidics to Every Lab?—A Systematic Review. *Micromachines* **2021**, *12*, 339. [[CrossRef](#)]
41. Guerra, M.; Volpone, C.; Galantucci, L.; Percoco, G. Photogrammetric measurements of 3D printed microfluidic devices. *Addit. Manuf.* **2018**, *21*, 53–62. [[CrossRef](#)]
42. Burke, I.; Assies, C.; Kockmann, N. Rapid prototyping of a modular optical flow cell for image-based droplet size measurements in emulsification processes. *J. Flow Chem.* **2024**, *14*, 515–528. [[CrossRef](#)]
43. Höving, S.; Ronnewinkel, P.; Kockmann, N. From Batch to Continuous Small-Scale Production of Particles: Mixer Design Methodology for Robust Operation. *Crystals* **2024**, *14*, 398. [[CrossRef](#)]
44. Dinter, R.; Willems, S.; Nissalk, T.; Hastürk, O.; Brunschweiler, A.; Kockmann, N. Development of a microfluidic photochemical flow reactor concept by rapid prototyping. *Front. Chem.* **2023**, *11*, 1244043. [[CrossRef](#)]
45. Meinel, C. *Design Thinking*; Springer: Berlin/Heidelberg, Germany, 2011.
46. Battat, S.; Weitz, D.A.; Whitesides, G.M. An outlook on microfluidics: The promise and the challenge. *Lab Chip* **2022**, *22*, 530–536. [[CrossRef](#)]
47. Wang, J.; Shao, C.; Wang, Y.; Sun, L.; Zhao, Y. Microfluidics for Medical Additive Manufacturing. *Engineering* **2020**, *6*, 1244–1257. [[CrossRef](#)]
48. Kockmann, N. Modular Equipment for Chemical Process Development and Small-Scale Production in Multipurpose Plants. *ChemBioEng Rev.* **2015**, *3*, 5–15. [[CrossRef](#)]
49. Gong, H.; Bickham, B.P.; Woolley, A.T.; Nordin, G.P. Custom 3D printer and resin for 18  $\mu\text{m}$   $\times$  20  $\mu\text{m}$  microfluidic flow channels. *Lab Chip* **2017**, *17*, 2899–2909. [[CrossRef](#)]
50. Ahmadianyazdi, A.; Miller, I.J.; Folch, A. Tunable resins with PDMS-like elastic modulus for stereolithographic 3D-printing of multimaterial microfluidic actuators. *Lab Chip* **2023**, *23*, 4019–4032. [[CrossRef](#)]
51. Schittecatte, L.; Geertsen, V.; Bonamy, D.; Nguyen, T.; Guenoun, P. From resin formulation and process parameters to the final mechanical properties of 3D printed acrylate materials. *MRS Commun.* **2023**, *13*, 357–377. [[CrossRef](#)]
52. Catterton, M.A.; Montalbino, A.N.; Pompano, R.R. Selective Fluorination of the Surface of Polymeric Materials after Stereolithography 3D Printing. *Langmuir* **2021**, *37*, 7341–7348. [[CrossRef](#)]
53. Oldach, B.; Wintermeyer, P.; Kockmann, N. Transfer of Periodic Phenomena in Multiphase Capillary Flows to a Quasi-Stationary Observation Using U-Net. *Computers* **2024**, *13*, 230. [[CrossRef](#)]
54. Oldach, B.; Chiang, Y.Y.; Ben-Achour, L.; Chen, T.J.; Kockmann, N. Performance of different microfluidic devices in continuous liquid-liquid separation. *J. Flow Chem.* **2024**, *14*, 547–557. [[CrossRef](#)]
55. Bacha, T.W.; Manuguerra, D.C.; Marano, R.A.; Stanzione, J.F. Hydrophilic modification of SLA 3D printed droplet generators by photochemical grafting. *RSC Adv.* **2021**, *11*, 21745–21753. [[CrossRef](#)] [[PubMed](#)]

**Disclaimer/Publisher’s Note:** The statements, opinions and data contained in all publications are solely those of the individual author(s) and contributor(s) and not of MDPI and/or the editor(s). MDPI and/or the editor(s) disclaim responsibility for any injury to people or property resulting from any ideas, methods, instructions or products referred to in the content.